

Review

Pt-Ni Nanoalloys for H₂ Generation from Hydrous Hydrazine

Liu Zhou ¹, Xianjin Luo ², Lixin Xu ^{1,2,3}, Chao Wan ^{1,2,3,4,*}  and Mingfu Ye ^{1,2,3,*}

¹ Hexian Chemical Industrial Development Institute, Engineering Research Institute, School of Chemistry and Chemical Engineering, Anhui University of Technology, Ma'anshan 243002, China; iLiu97@hotmail.com (L.Z.); lxxu@hotmail.com (L.X.)

² Anhui Haide Chemical Technology Co., Ltd., Ma'anshan 243002, China; AHUT.XJLuo@outlook.com

³ Ahut Chemical Science & Technology Co., Ltd., Ma'anshan 243002, China

⁴ College of Chemical and Biological Engineering, Zhejiang University, Hangzhou 310027, China

* Correspondence: wanchao1219@hotmail.com (C.W.); yehmf@iccas.ac.cn (M.Y.);

Tel.: +86-555-231-1807 (C.W.); +86-555-231-1551 (M.Y.)

Received: 29 June 2020; Accepted: 10 August 2020; Published: 13 August 2020



Abstract: Hydrous hydrazine (N₂H₄·H₂O) is a candidate for a hydrogen carrier for storage and transportation due to low material cost, high hydrogen content of 8.0%, and liquid stability at room temperature. Pt and Pt nanoalloy catalysts have been welcomed by researchers for the dehydrogenation of hydrous hydrazine recently. Therefore, in this review, we give a summary of Pt nanoalloy catalysts for the dehydrogenation of hydrous hydrazine and briefly introduce the decomposition mechanism of hydrous hydrazine to prove the design principle of the catalyst. The chemical characteristics of hydrous hydrazine and the mechanism of dehydrogenation reaction are briefly introduced. The catalytic activity of hydrous hydrazine on different supports and the factors affecting the selectivity of hydrogen catalyzed by Ni-Pt are analyzed. It is expected to provide a new way for the development of high-activity catalysts for the dehydrogenation of hydrous hydrazine to produce hydrogen.

Keywords: hydrous hydrazine; dehydrogenation; Pt nanoalloys; support

1. Introduction

Hydrogen energy, as a kind of green energy with abundant reserves, wide sources, and high energy density, has shown an excellent application prospect in fuel cells and as a substitute for fossil fuels [1–4]. In the process of utilization, it is a key to storage and transportation [5,6]. Hydrogen storage methods can be roughly divided into physical methods [7,8] and chemical methods [9,10], which have made some progress in a certain extent. Based on the liquid organic hydride, hydrogen storage technology in chemical methods, owing to large hydrogen storage capacity, high energy density, and safe and convenient liquid storage and transportation [11–13], has attracted the attention of scholars. The chemical nature of hydrazine (N₂H₄) is relatively active and can react with strong oxidants. However, hydrazine is likely to explode if it is left in the air for a long time or under high temperature heating. Therefore, hydrazine is an extremely dangerous substance and is not suitable as a hydrogen storage material [14,15], but hydrous hydrazine (N₂H₄·H₂O), as a liquid hydrogen storage material with excellent hydrogen storage content (8.0 wt%)—the only by-product when completely decomposed is N₂, which has no pollution to the environment—has always been considered to have great prospects [16–19].

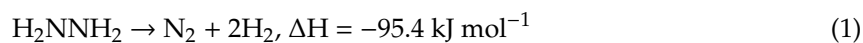
The decomposition process of hydrous hydrazine is often accompanied by side reactions that produce ammonia, which greatly reduces the hydrogen production efficiency of hydrous hydrazine [20].

Therefore, the development of a high catalytic rate and a high selectivity catalyst is the key to the actual production and application of hydrous hydrazine. Many studies have shown that the Pt-based catalyst has excellent performance in the decomposition of hydrous hydrazine [21–24]. However, the scarcity of precious metal resources and the high price has limited its large-scale industrial application [25,26]. Therefore, the addition of the second component active metal is necessary, which can affect the structural properties of the catalyst, and thus affect the stability of the catalyst. Combining Pt with other metals can effectively change its surface properties to obtain better catalytic performance, and bimetallic catalysts can combine the high activity and stability of precious metal catalysts with the price advantages of other particles [27]. For the hydrogen production reaction of hydrous hydrazine, in the literature that has been reported so far, the Ni-Pt bimetallic catalyst [28–30] has the best catalytic effect. The commonly used supports for hydrous hydrazine dehydrogenation catalysts are metal oxide supports, such as CeO₂ [31–33], Al₂O₃ [34,35], and TiO₂ [36,37]. The role of the support in the catalyst is often overlooked, but for hydrous hydrazine dehydrogenation reaction, the carrier is very important for its catalytic performance effect.

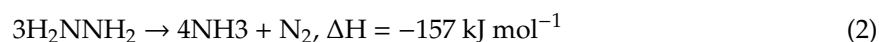
Herein, we review a general overview of Pt nanoalloy catalysts for hydrous hydrazine reduction and introduce the decomposition mechanism of hydrazine to illustrate the design principle of the catalyst. The catalytic activity of hydrous hydrazine on different supports and the factors affecting the selectivity of hydrogen catalyzed by Ni-Pt are analyzed. This article mainly reviews the research progress of Ni-Pt catalysts for hydrous hydrazine hydrogen production, introduces the hydrazine decomposition reaction and the principle of hydrazine hydride decomposition hydrogen production, and discusses in detail the research status of different kinds of hydrous hydrazine Ni-Pt catalysts for hydrogen production. We hope to provide a new way for the development of excellent catalysts for the decomposition of hydrous hydrazine.

2. Mechanism of H₂ Production from Hydrous Hydrazine through Pt Nanoalloys

The reaction pathway of hydrous hydrazine [38] depends on the breaking of the N–N bond and N–H bond. In theory, the N–N bond energy is 286 KJ mol^{−1} and the N–H bond total cleavage energy is 360 KJ mol^{−1} [39]. Thus, the N–N bond seems to be more easily fractured. However, if N₂H₄ breaks down to N₂H₂ and H₂, the N–H bond energy is 276 KJ mol^{−1}, and the H-metal bond energy is stronger than the N–metal bond, which makes the N–H bond more likely to break. Zhang's team [40] summarized most of the literature on the decomposition of N₂H₄ and proposed a relatively complete mechanism of N₂H₄ (Figure 1). The effective hydrogen storage component of hydrous hydrazine is hydrazine (N₂H₄), and its decomposition reaction can be carried out according to the following two competitive paths [41,42]: complete decomposition,



and incomplete decomposition,



from the application of hydrogen storage, it is necessary to selectively promote the complete decomposition of N₂H₄ into H₂ and N₂, and effectively inhibit the formation of NH₃ by-products. The key to the development of N₂H₄·H₂O controllable hydrogen technology lies in the development of cheap catalysts with high catalytic activity and high hydrogen production selectivity [43].

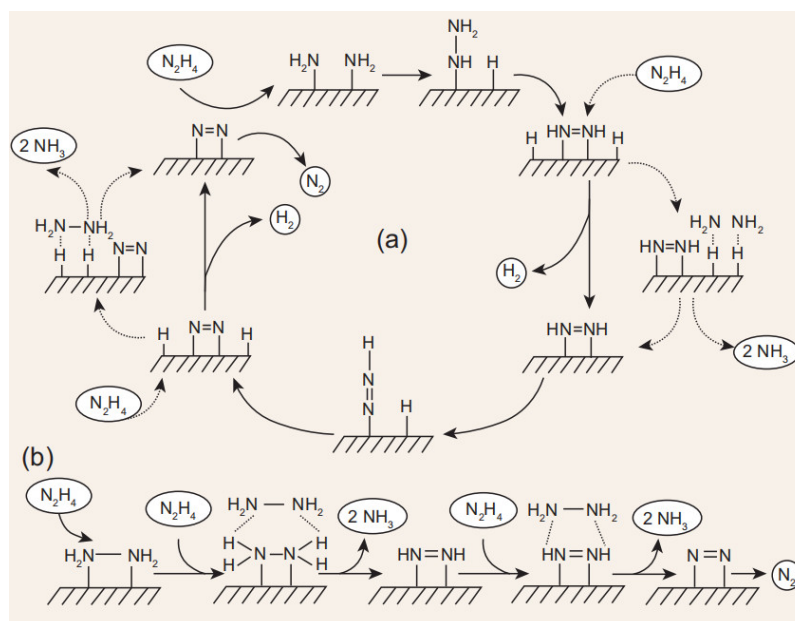


Figure 1. Reaction pathways for hydrazine decomposition. (a) NH_3 , N_2 , and H_2 formation. (b) NH_3 and N_2 formation; copyright (2017), *National Science Review*.

Early studies focused on the mechanism of adsorption on the surfaces of Ir [44], Pt [45,46], and Rh [47,48] model metals. For hydrogen production from hydrous hydrazine, changing the order of the rupture of $\text{N}-\text{N}$ and $\text{N}-\text{H}$ bonds is the main strategy to change the selectivity. Transition metals (such as Ir, Ru, and Ni) are the most effective $\text{N}-\text{H}$ bond activation candidates in various catalytic systems and exhibit high hydrazine decomposition activity under mild conditions. Nevertheless, the selectivity of H_2 is limited to less than 10% as compared to Ru and Ir catalysts [49]. So far, single-metal catalysts have failed to achieve complete catalytic decomposition from hydrazine to H_2 without forming NH_3 . The Pt-based catalysts have strong catalytic activity [50]. Therefore, the modification of the catalyst is necessary to improve the selectivity of H_2 . Bimetallic catalysts, due to their unique electronic and chemical properties, exhibit enhanced activity, selectivity, and stability compared with the parent metals. For Pt-promoted nickel catalysts, the results of x-ray diffraction (XRD) in Zhang's experiment [40] showed that the main diffraction peaks only show the presence of Ni. The shift of the diffraction peak to a smaller angle after the substitution of Pt indicates that the co-reduction of Ni-Pt with the second metal in the bimetallic catalyst further confirms the formation of Ni-Pt alloy, as indicated by temperature programmed reduction (TPR) data. In addition, the results of x-ray absorption fine structure (EXAFS) experiments with extended x-ray show that most Pt species exist in Ni-Pt alloys, which leads to electron transfer from Ni to Pt.

3. Ni-Pt Nanoalloying

In the past reports, many transition metal nano-catalysts have been synthesized by co-precipitation [51], chemical reduction, combustion synthesis [52], galvanic displacement [53], impregnation [54], and alloying [55]. Among them, alloying is an effective strategy to improve catalytic activity and hydrogen selectivity [55]. Fixing the catalyst nanoparticles on the basic carrier can not only improve the durability of the catalyst, but also improve the selectivity of hydrogen [56]. Compared with the corresponding single-metal, nanoalloys have the advantages of reconfigurable electronic structure, variable composition ratio, and adjustable selectivity, which show unique properties different from bulk alloy and metal elements [56]. Because of the nano-size effect and a large number of kinks, the nanoalloy obtains higher specific surface energy and rich active sites through electronic configuration reorganization, which greatly promotes its catalytic performance, further evidence that

it has obvious superiority and broad application prospects in chemical catalysis. On the one hand, nanoalloy catalytic materials cannot only catalyze the reforming of syngas, but also catalyze various coupling reactions, which has promoted the development of chemical industry, energy, environment, medicine, and other industries. Nanoalloy catalytic materials cannot only enhance the activity through the surface structure, but also improve the performance through the mechanical effect, greatly enriching the theoretical system of nano-catalysis [57]. The nanoalloys (NAs) are obviously different from bulk alloy or single-metal, with tunable composition and proportion, variable structure, reconfigurable electrical characteristic structure, and optimized performance, which give NAs a fascinating prospect in the field of catalysis.

Based on the previously reported literature, we found that most of the papers were based on the dehydrogenation of hydrous hydrazine on different supports supported with different proportions of Ni-Pt bimetallic catalysts [58–60]. The noble metal Pt has high reduction potential and stability, so it is easier to prepare new structures [61]. They provide excellent catalytic properties that are closely related to Fermi's electrons. The base metal, Ni, readily gives up electrons and is oxidized to a lower reduction potential. Ni is one of the most important catalysts for industrial catalysis because of its excellent catalytic selectivity and cost efficiency [62]. Compared with the single-metal, the activity and stability of the Pt-Ni catalyst were improved significantly [57]. Figure 2 shows the etching mechanism of Pt-Ni nanoparticles (NPs). Noble/base metal-mixed NAs (NBMNAs) [63–65] are promising catalysts that combine the high catalytic activity of noble metal Pt and the high selectivity of base metal Ni. At the same time, a high utilization ratio of noble metal atoms can be obtained. The electronic structures of Pt and Ni are reorganized by alloying, which is an effective way to reduce the irreversible oxidation or leakage of base metals and to improve the stability of catalysts. The proper distribution of metal elements helps to form the Pt surface layer of noble metals to protect the catalysts. At the same time, the performance of the catalyst is improved because of the mechanical action of the alloy base and the precious metal.

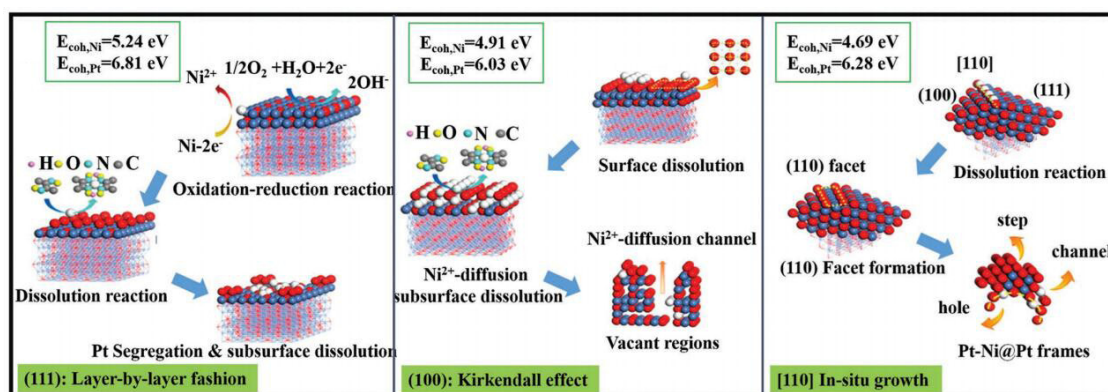


Figure 2. Galvanic replacement; copyright 2014, American Chemical Society.

4. Hydrous Hydrazine

Hydrogen storage materials with a large energy storage density are the radical condition for practical application; in the required temperature range, the energy hydrogen storage density of a large number of metal alloy hydrogen storage materials and physical adsorption materials studied in the past can hardly meet the demand of practical application [66]. Therefore, in recent years, light-weight hydrogen storage substances with ultra-high hydrogen storage capacity have become a research hotspot.

In liquid phase hydrogen storage carriers, hydrous hydrazine has been widely studied by scholars because of outstanding hydrogen storage density, easy storage and transportation, and convenient use N_2H_4 . There are two decomposition paths for N_2H_4 : complete decomposition to produce H_2 and N_2 , and incomplete decomposition to produce N_2 and NH_3 . The former reaction path produces H_2 for

human use, while the latter produces NH_3 that can poison Nafion membranes and fuel cell catalysts, so the latter reaction must be avoided. So far, the catalytic decomposition of hydrous hydrazine has reached 100% catalytic selectivity [67–71]. The catalytic kinetic is still very slow, which enormously blocks the practical application of the system. Thence, it is urgent to develop highly selective and efficient catalysts at room temperature.

Hence the decomposition of hydrous hydrazine tends to produce NH_3 rather than H_2 , which not only reduces the yield of hydrogen, but also complicates the separation process due to the low toxicity of Nafion membrane and the fuel cell catalyst to NH_3 [72–74]. Therefore, it is of great significance to develop a highly efficient and selective hydrous hydrazine catalyst for hydrogen evolution. In recent years, metal nano-catalysts have made great progress in the catalytic decomposition of hydrous hydrazine. The Ir/ Al_2O_3 catalyst was the first reported active catalyst for the decomposition of hydrous hydrazine catalyzed by highly dispersed metal particles [75]. In order to develop high-property catalysts for hydrogen-selective dehydrogenation of hydrous hydrazine, bimetallic alloys based on nickel and noble metals Rh, Pt, or Ir can completely decompose hydrous hydrazine to produce hydrogen selectively [76–79]. The H_2 selectivity of bimetallic NPs is strongly dependent on the metal ratio, and the alloy nano-catalyst with stable surface activity can achieve 100% hydrogen selectivity, which is more active than the corresponding single-metal nano-catalyst [80]. It is reasonable to consider that the coordination in bimetallic catalysts can adjust the bond mode of reactants, stabilize the reaction intermediates on the catalyst surface, and improve the catalytic activity and stability. These bimetallic nano-catalysts have good hydrogen selectivity for the dehydrogenation of hydrous hydrazine, but the chemical kinetics are still exceedingly low [81].

5. H_2 Selectivity in Hydrous Hydrazine Dehydrogenation

Although bimetallic nano-catalysts have a good hydrogen selectivity for the decomposition of hydrous hydrazine, chemical kinetics are still intensely low [82]. In subsequent studies, Zhu et al. [83] found that the presence of basic additives, such as NaOH, was beneficial to increase the catalytic activity and selectivity of metal catalysts for hydrogen production from hydrous hydrazine. When NaOH is added at 0.5 M, the selectivity of $\text{Ni}_{45}\text{Pt}_{55}$ increases from 61% to 86%, and the selectivity of $\text{Ni}_{50}\text{Ir}_{50}$ increases from 7% to 95% at 25 °C [84]. The alkaline solution makes the surface of the catalyst highly alkaline, which helps to inhibit the formation of alkaline selectivity, and thus favors the formation of H_2 . In addition, with the increase of the reaction temperature, the catalytic performance is significantly improved [85]. In the presence of NaOH, highly dispersed surfactant Ni-Pt NPs were synthesized, in which NaOH plays an important role in the formation and stability of small-size NPs. The crystalline porous structure of metal organic frameworks (MOFs) can restrict the migration and aggregation of metal NPs. The MOF-supported bimetallic NPs [86] have recently been reported as the catalysts of high properties for the selective decomposition of hydrazine.

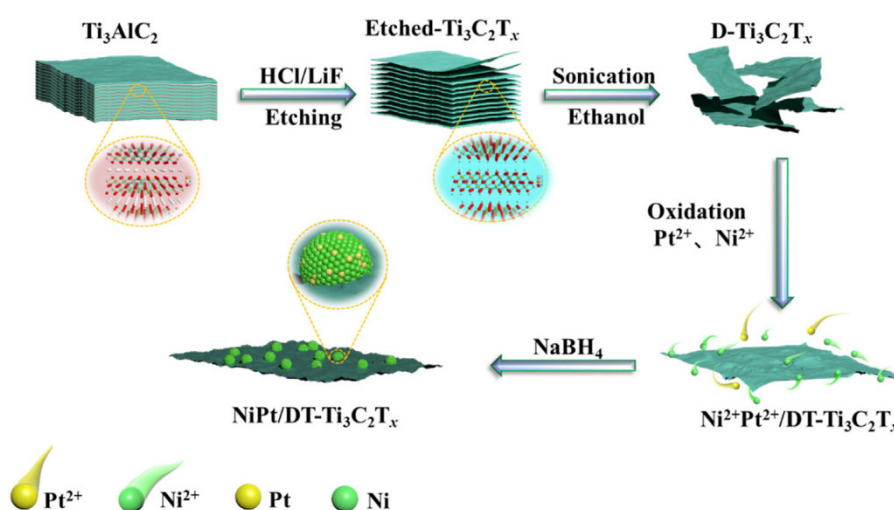
6. Catalytic Effect of Different Supports on Hydrous Hydrazine

Extensively used industrial heterogeneous catalysts are usually composed of metal nanoparticles supported on a large surface area. In recent decades, with the discovery of metal-carrier interactions, the significance of the oxides has been recognized to an increasing extent. Apart from dispersing metal particles, oxide supports also play a role in influencing the catalytic performance of metal catalysts through electronic or geometric effects. Representative oxides include CeO_2 , TiO_2 , and Fe_2O_3 . The strategies to further improve its performance, including the choice of metal composition and the adjustment of metal-carrier interaction, have been analyzed [87]. In heterogeneous catalysis, support in the nano-catalyst may play a key role in the whole process. On the one hand, support can be used to disperse and reduce the size of the metal nanoparticles during the synthesis process, thereby exposing more active sites and leading to the improvement of catalytic performance. On the other hand, coupling metal nanoparticles with a support may introduce additional synergistic effects, so inherently changing

the physical and chemical properties of the interface between them. Therefore, the catalytic activity and selectivity can be adjusted by changing different supports.

6.1. TiO_2 -Decorated $Ti_3C_2T_x$

In 2020, Ni-Pt nanoparticles (NPs) dispersed on TiO_2 -decorated $Ti_3C_2T_x$ (denoted as DT- $Ti_3C_2T_x$) nanosheets were prepared (Lu et al.) [88] by a facile wet chemical reduction method and used as an effective catalyst for dehydrogenation of N_2H_4 as shown in Scheme 1. The oxygen-rich functional groups on the surface of DT- $Ti_3C_2T_x$ not only contributed to the formation and fixation of monodisperse Ni-Pt NPs, but also enhanced the synergy between metal NPs and the MXene carrier. In all the tested samples, the best $Ni_{0.8}Pt_{0.2}/DT-Ti_3C_2T_x$ nano-catalyst showed 100% H_2 selectivity and the optimal catalytic performance. The turnover frequency (TOF) value of the selective dehydrogenation of N_2H_4 at 323 K was 1220 h^{-1} . Ni-Pt alloy NPs were evenly dispersed on DT- $Ti_3C_2T_x$ nanosheets with an average size of 2.8 nm. DT- $Ti_3C_2T_x$ in Ni-Pt/DT- $Ti_3C_2T_x$ acts as an electron donor for Ni-Pt NPs to enhance the electron density of Ni-Pt NPs. Appropriate oxidation of $Ti_3C_2T_x$ MXene can augment the number of oxygen-containing functional groups on the surface of $Ti_3C_2T_x$, which plays an important role in fixing the small particle size Ni-Pt NPs and promoting the synergy between Ni-Pt NPs and DT- $Ti_3C_2T_x$. The Ni-Pt/DT- $Ti_3C_2T_x$ catalyst shows strong activity, 100% H_2 selectivity, and excellent durability in the production of hydrogen from hydrazine and hydrazinoborane in aqueous solution. In addition, DT- $Ti_3C_2T_x$ supports other bimetallic NPs and also shows splendid catalytic activity, emphasizing the generality of DT- $Ti_3C_2T_x$ as a carrier.



Scheme 1. Schematic diagram for the preparation of Ni-Pt/DT- $Ti_3C_2T_x$; copyright (2020), Elsevier.

6.2. CeO_2

In 2018, Luo et al. [89] reported excellent catalytic properties for the co-reduction composite of Ni-Pt nanoparticles supported on CeO_2 nanospheres and the generation of hydrogen from hydrazine basic solutions at ambient temperature. As can be seen from Figure 3a, Ni- CeO_2 has almost no catalytic activity. However, when Ni- CeO_2 is alloyed with Pt, Ni-Pt- CeO_2 catalysts with different metal ratios show strong catalytic activity and selectivity. As can be seen from Figure 3b, the dehydrogenation effect of the Ni-Pt alloy catalyst on hydrous hydrazine is different with different supports, and the catalytic performance of Ni-Pt- CeO_2 is the best, which indicates that the CeO_2 nanosphere is one of the key factors to promote the catalytic performance. Through the interaction between Ni-Pt and CeO_2 , the $Ni_5Pt_5-CeO_2$ catalyst has remarkable catalytic activity, 100% hydrogen selectivity, and hydrazine dehydrogenation selectivity, and the TOF value is 416 h^{-1} at room temperature.

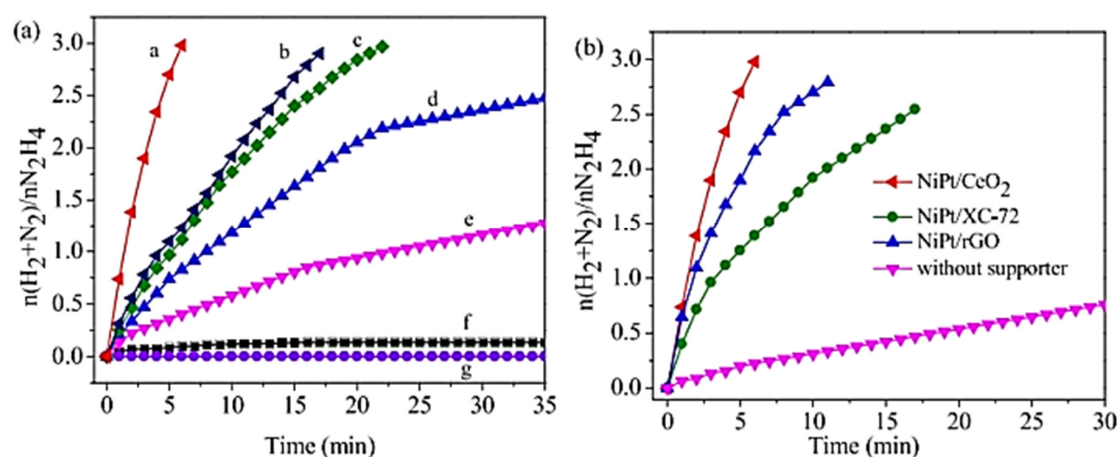
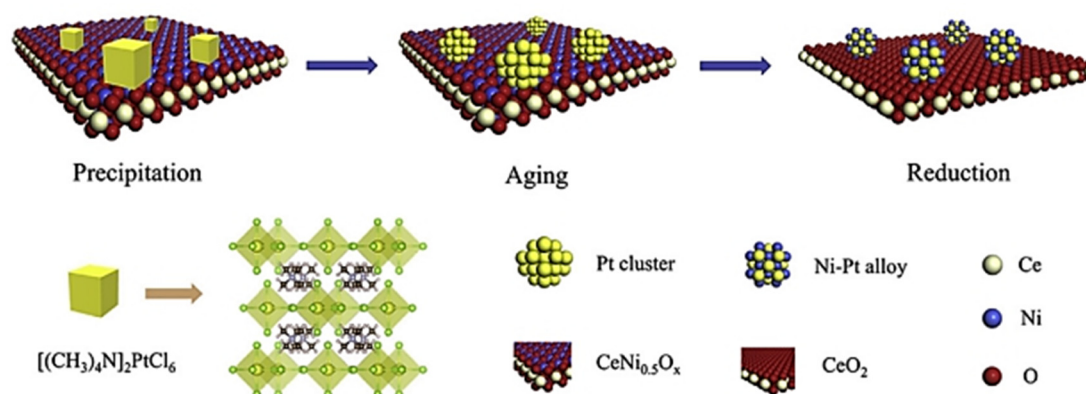


Figure 3. (a) Catalytic performance tests of the Ni-Pt-CeO₂ catalyst with different molar ratios of metal in the presence of 0.75 mol/L NaOH at 298 K (a, b, c, d, e, f, and g represent the Ni₅Pt₅-CeO₂, Ni₇Pt₃-CeO₂, Ni₃Pt₇-CeO₂, Ni₁Pt₉-CeO₂, Ni₉Pt₁-CeO₂, Ni-CeO₂, Pt-CeO₂). (b) Catalytic performance of Ni₅Pt₅ on different supporters toward the decomposition of hydrazine at 298 K; copyright (2018), Elsevier.

Wang et al. [90] prepared the Ni₅₀Pt₅₀/CeO₂ catalyst, as shown in Scheme 2, in 2019 and then transferred it to a sealed polytetrafluoroethylene-lined autoclave for aging treatment. Under an H₂ atmosphere, the resulting black sediment is finally reduced at a high temperature to obtain a tar electronic catalyst. According to ICP-AES elemental analysis, the actual composition of the target Ni₅₀Pt₅₀/CeO₂ catalyst is 50.3 mol% Ni_{50.4}Pt_{49.6}/49.7 mol% CeO₂, which is close to the originally designed atomic ratio. In order to better understand the phase evolution of the catalyst during preparation, they combined phase/microstructure/chemical state analysis of samples collected at different stages. It was found that the preparation of the catalyst involved the structure of [(CH₃)₄N]₂PtCl₆ and CeNi_{0.5}O_x in the coprecipitation step and their evolution in the consecutive reduction and aging process. Preventing [(CH₃)₄N]₂PtCl₆ corrosion of metal Pt during aging is an essential procedure in the preparation process. It has a profound impact on the cracking performance of the catalyst on the composition, microstructure characteristics, and corresponding catalyst of metal Pt. Their study clearly describes for the first time the phase/structure evolution during the preparation of Ni₅₀Pt₅₀/CeO₂ catalyst. This may lay the foundation for future rational design and control of the synthesis of high-performance catalysts to promote the production of chemical hydrides such as N₂H₄·H₂O.



Scheme 2. Schematic illustration of the preparation process of Ni₅₀Pt₅₀/CeO₂ catalyst by co-precipitation method; copyright (2019), Elsevier.

A simple impregnation-reduction method was used to prepare a monolithic catalyst consisting of Ni-Pt/CeO₂ nanoparticles and granular activated carbon (GAC) by Wang et al. [91] in 2018, as shown in

Figure 4. The study found that the catalyst activity, H_2 selectivity, and atmosphere can be easily adjusted by transforming the annealing temperature. The optimum Ni-Pt/CeO₂/GAC catalyst can completely decompose $N_2H_4 \cdot H_2O$ into H_2 in the presence of 1M NaOH at moderate temperature, with 100% selectivity. Significantly, by utilizing this monolithic catalyst, they have formed an $N_2H_4 \cdot H_2O$ -based H_2 generation (HG) system with a material hydrogen capacity of up to 6.54 wt%.



Figure 4. The system composed of a concentrated $N_2H_4 \cdot H_2O$ solution and a high-performance monolithic catalyst yielded a hydrogen capacity of 6.54 wt%, which is promising for on-board application; copyright (2018), *American Chemical Society*.

6.3. Al_2O_3

In 2012, Pt-modified Ni/ Al_2O_3 catalysts were synthesized by Zhang et al. [92] and studied in the dissociation of hydrous hydrazine, as shown in Figure 5. Compared to Ni/ Al_2O_3 , TOF was found to be 7 times stronger in Ni-Pt, and the selectivity to H_2 was improved to 98%. The results show that the formation of Pt-Ni alloy weakens the adsorption state, including the interaction between H_2 and NH_x and Ni atoms on the surface. On the Ni-Pt_x/ Al_2O_3 catalyst, the weakening effect can explain the increase of reaction rate and H_2 selectivity.

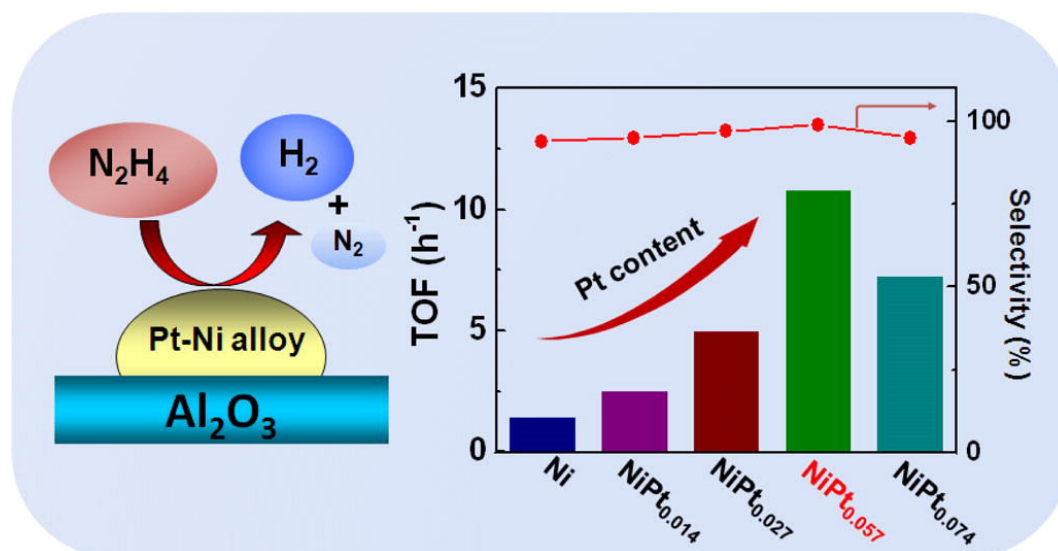


Figure 5. Catalytic performance tests of the Ni-Pt- Al_2O_3 catalyst with different molar ratios of metal in the presence of Ni, Ni-Pt_{0.014}, Ni-Pt_{0.027}, Ni-Pt_{0.057}, and Ni-Pt_{0.074}; copyright (2012), *Elsevier*.

6.4. Graphene Oxide (GO)

In 2018, Xu et al. [93] used the wet chemical reduction method, as shown in Figure 6a, to fix the ultrafine and uniform dispersion bimetallic Pt-Ni nanoparticles (NPs) onto a new three-dimensional N-doped graphene network (NGNs), which was fabricated by cross-linking graphene oxide (GO) with melamine-formaldehyde resin (MFR) and N-dope graphene layers. As can be seen from Figure 6b, the scanning electron microscope of NGNs-850 and Pt_{0.5}Ni_{0.5} NGNs-850 showed a porous 3D structure with randomly opened stomatal layers. The evenly dispersed Pt_{0.5}Ni_{0.5} NPs on NGNs-850 can be seen from the transmission electron microscope (TEM) and high-angle annular dark-field scanning image of Pt_{0.5}Ni_{0.5} NPs on Figure 6c–f Pt_{0.5}Ni_{0.5}/NGNs-850. The average particle size is 2.2 nm. The main purpose of this work is to show that the prepared Pt_{0.5}Ni_{0.5}/NGNs-850 catalyst has very high catalytic activity for hydrous hydrazine to produce hydrogen, and its catalytic activity is 943 h⁻¹ at 303 K. The high property of the catalyst is mainly due to the ultra-small size effect, the powerful synergy between Pt and Ni atoms, as well as the excellent porous structure of the 3D network. This was achieved by increasing the interaction between the graphene surface and the metallic species through N-bonding and graphene cross-linking.

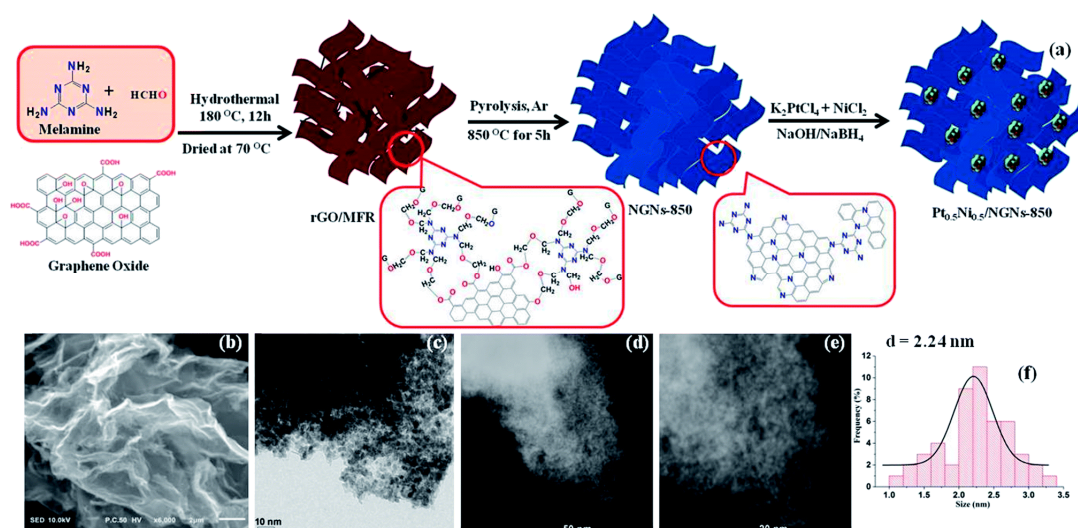


Figure 6. (a) Schematic illustration for the synthesis of 3D nitrogen-doped graphene networks (NGNs-850) and Pt_{0.5}Ni_{0.5}/NGNs-850, (b) SEM image displaying the 3D framework of Pt_{0.5}Ni_{0.5}/NGNs-850, (c) the transmission electron microscope (TEM) and (d) and (e) high-angle annular dark-field scanning microscope (HAADF STEM) images showing the presence of ultra-fine and highly dispersed Pt-Ni nanoparticles (NPs) in Pt_{0.5}Ni_{0.5}/NGNs-850, and (f) the corresponding size histograms of Pt-Ni NPs in Pt_{0.5}Ni_{0.5}/NGNs-850; copyright (2018), *Journal of Materials Chemistry A*.

In 2020, Lu et al. [94] reported a low Ni-Pt-containing bimetallic catalyst immobilized on a new MIL-101/rGO composite prepared by a simple and easy impregnation-reduction method (Figure 7). It was discovered that the synthesized Ni-Pt/MIL catalyst has the best catalytic performance and 100% hydrogen selectivity for the hydrogen evolution of hydrous hydrazine at 323 K alkalinity. The turnover frequency value (TOF) is 960 h⁻¹. In addition, the Ni-Pt/MIL catalyst also shows excellent durability.

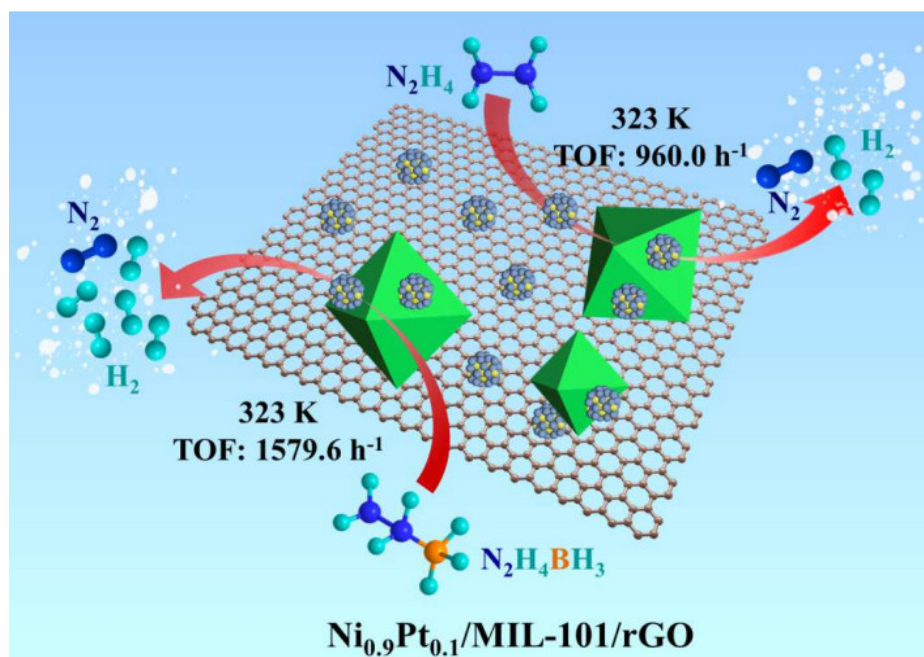
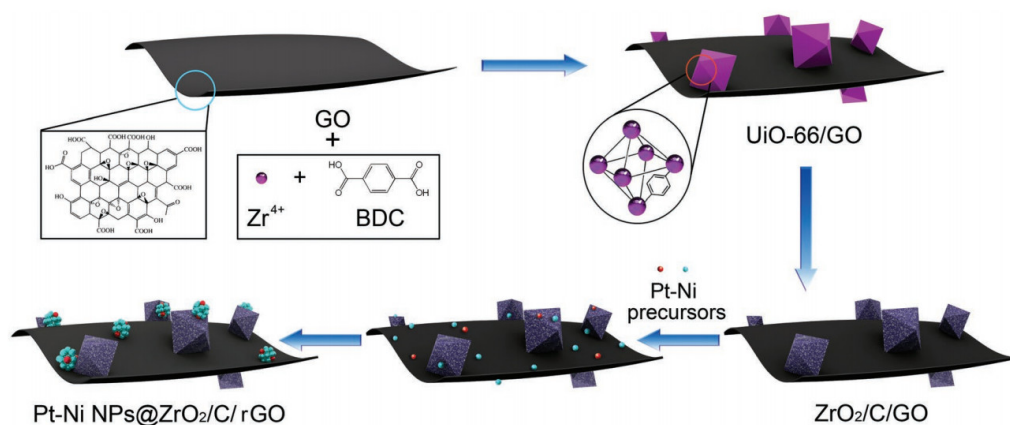


Figure 7. A low Pt-containing Ni-Pt nano-catalyst immobilized on a metal organic framework (MOF)/rGO composite has been synthesized for hydrogen production from hydrous hydrazine and hydrazine borane; copyright (2020), Elsevier.

Xu et al. [95] fixed the ultrafine bimetallic Pt-Ni nanoparticles (NPs) with an average size of 1.8 nm to zirconia/porous carbon/graphene oxide ($ZrO_2/C/rGO$) by the wet chemical reduction method using the template for a metal-organic skeleton shown in the Scheme 3. Unexpectedly, hydrogen is generated from hydrazine, and an extremely high turnover frequency value can be provided to 1920 h^{-1} at 323 K. The high enhanced catalytic activity can be attributed to the small size effect, the strong synergistic effect between Pt and Ni atoms, and the strong metal-support interaction.



Scheme 3. Schematic illustration for the immobilization of Pt-Ni NPs on the metal-organic framework template $ZrO_2/C/rGO$ support; copyright (2019), *Small Methods*.

Cheng et al. [96] have successfully synthesized ultrafine monodisperse Ni-Pt alloy NPs by conjugating nickel acetylacetonate and platinum acetylacetonate with borane-tert-butylamine (BTB) in $90\text{ }^\circ\text{C}$ oleylamine (Figure 8). The composition of Ni-Pt NPs is controlled by changing the initial molar ratio of the metal precursor. Ni-Pt NPs were deposited on graphene, and the catalytic dehydrogenation of hydrazine alkaline solution was tested under ambient conditions. Among all the tested catalysts, Ni₈₄Pt₁₆/graphene showed 100% hydrogen selectivity and had obvious high catalytic activity. The TOF

value at 50 °C was 415 h⁻¹ and the TOF value at 25 °C 133 h⁻¹, higher than most reported values. It is believed that the metal composition-controlled synthesis of ultrafine alloy NPs with a limited size distribution strongly promotes the practical application of aqueous hydrazine as a hydrogen storage material.

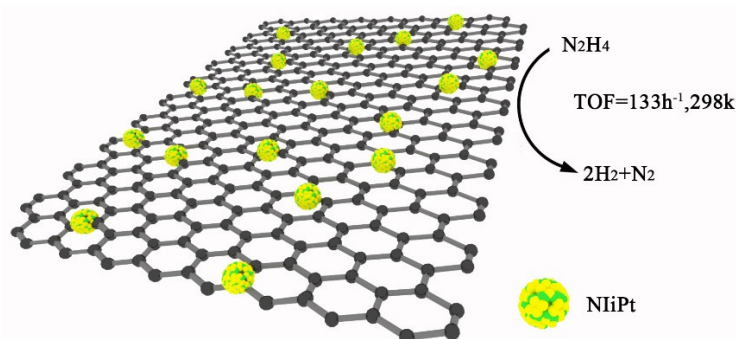


Figure 8. Ni₈₄Pt₁₆/graphene exhibited 100% hydrogen selectivity, and marked high catalytic activity, with turnover frequency (TOF) values of 415 h⁻¹ at 50 °C and 133 h⁻¹ at 25 °C for hydrogen generation from alkaline solution of hydrazine; copyright (2015), ACS Publications.

6.5. La₂O₃

Wang et al. [97] reported the catalytic decomposition of concentrated hydrous hydrazine solutions over La₂O₃-supported Ni-Pt alloy catalysts. The Ni-Pt/La₂O₃ catalyst synthesized by one-step coprecipitation method has high catalytic activity and 100% selectivity. In particular, their research demonstrated that a system consisting of concentrated N₂H₄·H₂O solutions, a high capability Ni-Pt/La₂O₃ catalyst, and an adequate amount of alkali accelerator can produce 6% of the material's hydrogenation capacity. As shown in Figure 9, the catalytic performance of the Ni-Pt/La₂O₃ catalyst is highly dependent on Pt content. The Pt/La₂O₃ catalyst was completely deactivated, and the Ni/La₂O₃ catalyst showed worse catalytic activity and moderate dehydrogenation selectivity. Compared with the Ni/La₂O₃ catalyst, the catalytic activity of the Ni-Pt/La₂O₃ catalyst with Pt/Ni Mole ratio of 1/9 was increased by 40 times, and the selectivity of H₂ was increased from 72% to 100%. When the molar ratio of Pt/Ni increased to 2/3, the catalyst showed the best catalytic property. In the presence of 3.0 M NaOH, it can completely decompose N₂H₄·H₂O in 1.5 min at 30 °C. Assuming that all the nickel atoms are involved in the catalytic reaction, the average reaction rate on the Ni₆₀Pt₄₀/La₂O₃ catalyst can reach 448 h⁻¹. Studies have shown that the best Ni₆₀Pt₄₀/La₂O₃ catalyst can complete the decomposition reaction of N₂H₄·H₂O in the presence of 3.0 M NaOH at 30 °C to generate hydrogen at a rate of 448 h⁻¹.

In this paper [98], the supported Ni@Ni-Pt La₂O₃ catalyst with core-shell structure was synthesized by coprecipitation and galvanic displacement method. The catalyst has high catalytic activity and 100% selectivity for hydrous hydrazine hydrogenation under mild conditions, which is superior to most reported hydrous hydrazine decomposition catalysts. The good catalytic performance of the Ni@Ni-Pt La₂O₃ catalyst is related to the electronic and geometric modification induced by Pt on the surface of the catalyst. When the reaction temperature was raised from 30 °C to 60 °C, the reaction rate increased about 6 times, as shown in Figure 10. Interestingly, there was no effect of the temperature on H₂ selectivity. The decomposition of N₂H₄·H₂O over the Ni@Ni-Pt La₂O₃ catalyst has 100% H₂ selectivity in the temperature range of 30–60 °C.

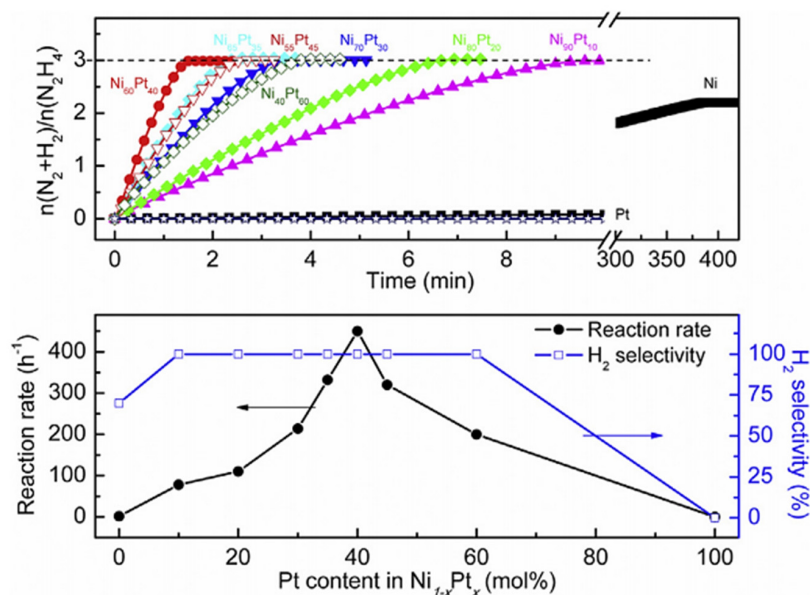


Figure 9. Time-course profiles (top) and Pt content dependence of the reaction rate and H₂ selectivity (bottom) of the system composed of 4 mL of 0.5 M N₂H₄·H₂O + 3 M NaOH solution and Ni_{1-x}Pt_x/La₂O₃ catalysts at 30 °C. The catalyst/N₂H₄·H₂O molar ratio was fixed at 1:10; copyright (2016), Elsevier.

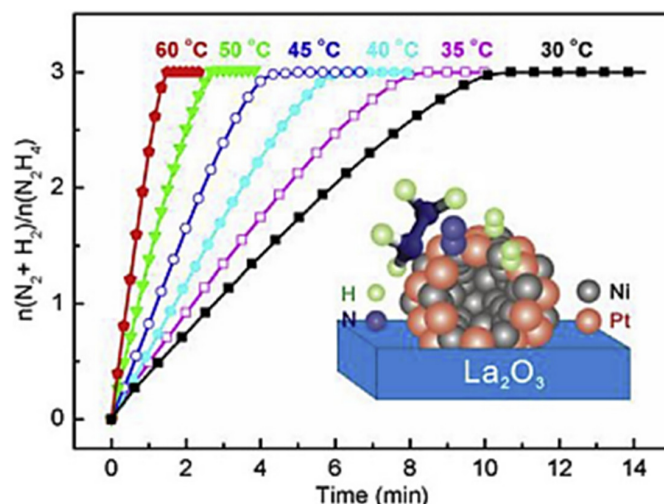
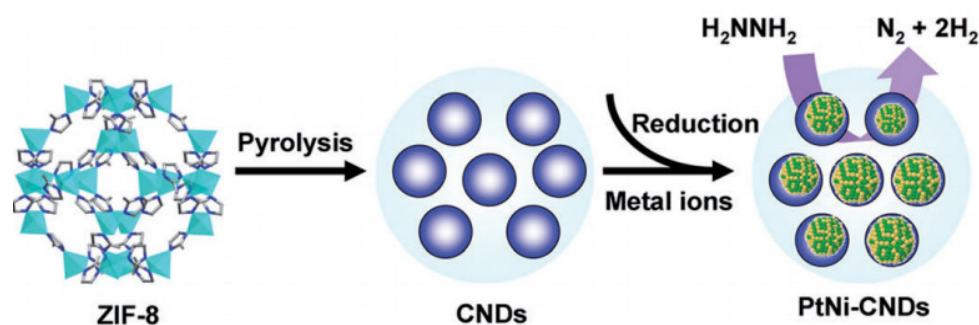


Figure 10. Decomposition kinetics curves of N₂H₄·H₂O over the Ni@NiPt/La₂O₃ catalyst (Pt/Ni molar ratio of 1/8) at varied temperatures. The catalyst/N₂H₄·H₂O molar ratio was fixed at 1:10; copyright (2015), Elsevier.

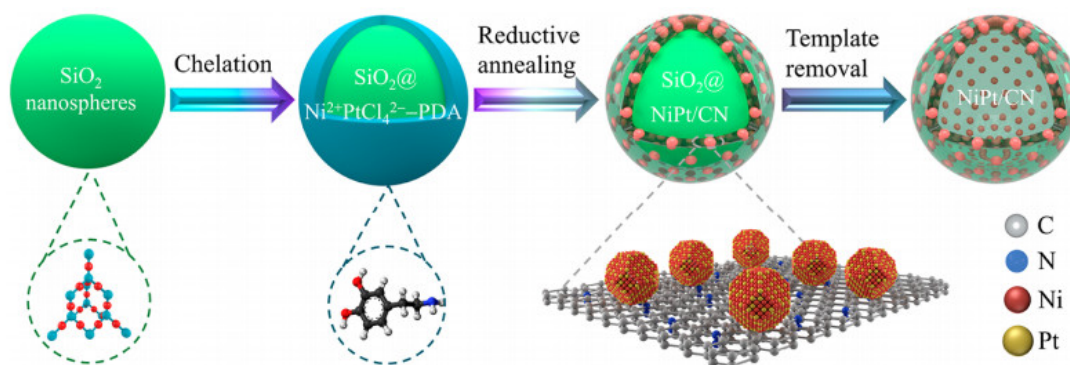
6.6. CN

Highly dispersed Pt-Ni nanoparticles (NPs) were synthesized on the surface of carbon nanodots (CNDs) with metal-organic framework ZIF-8 as a raw material [99] (Scheme 4). The obtained Pt-Ni-CND catalyst has 100% H₂ selectivity and distinguished activity for the decomposition of N₂H₄·H₂O at an ambient temperature. Carbon nanotubes (CNTs) were used as the support of NPs to promote the kinetics of electron transfer and mass transfer in the catalytic reaction. The introduction of water-soluble CNDs was able to effectively anchor NPs, control the small size of NPs, and guard against the aggregation in solution. Compared with the traditional water-soluble NPs, due to the lack of long-chain organic groups on CNDs, the NPs immobilized on CNDs have more catalytic sites for the contact between reactants and NPs. The results show that the synthesized NP-CND catalyst has high activity for hydrous hydrazine decomposition at room temperature.



Scheme 4. Schematic illustrations of the use of ZIF-8-derived carbon nanodots (CND) as supports to immobilize bimetallic NPs and their use as catalysts for the decomposition of hydrous hydrazine; copyright (2014), *ChemCatChem*.

In this paper [100], a layered nanostructure Ni-Pt/N-doped carbon peroxide is synthesized without three steps, which can solve these problems simultaneously (Scheme 5). N-doped carbon substrate and catalytic active Ni-Pt nanoparticles were formed by the chelation of metal precursors with dopamine and the thermal decomposition of the complexes in reducing atmosphere. Due to the use of silicon dioxide templates and dopamine precursors, the N-doped carbon substrate has a layered macroporous structure. This, coupled with the evenly dispersed tiny Ni-Pt nanoparticles on the carbon substrate, provides opportunities for rich and accessible activity. Because of these favorable properties, the Ni-Pt/N-doped carbon catalyst can completely and rapidly produce hydrogen in basic $\text{N}_2\text{H}_4 \cdot \text{H}_2\text{O}$ solution at 50°C at a rate of 1602 h^{-1} , which is superior to existing $\text{N}_2\text{H}_4 \cdot \text{H}_2\text{O}$ decomposition catalysts.

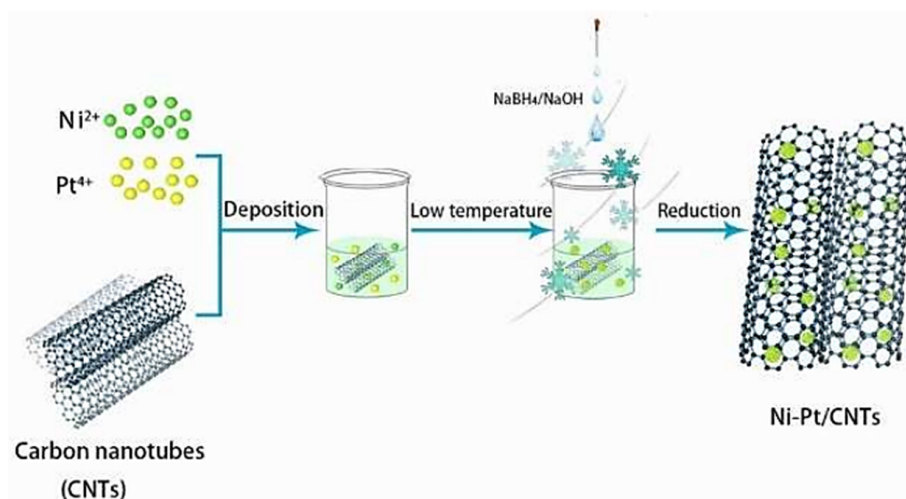


Scheme 5. Schematic diagram of the fabrication process of the Ni-Pt/NC nanocomposite catalyst; copyright (2020), *ACS Publications*.

In 2019, Wan et al. [101] designed a series of Ni-Pt/CNTs catalysts and prepared Ni-Pt/CNTs catalysts by wet chemical reduction method (Scheme 6). The crystal structure, chemical state, and morphology of the catalyst were characterized in detail. In these catalysts, $\text{Ni}_{0.4}\text{Pt}_{0.6}/\text{CNTs}$ have higher catalytic activity, a turnover frequency at 50°C of 1725.3 h^{-1} , and a low E_a of 36.3 KJ mol^{-1} . $\text{Ni}_{0.4}\text{Pt}_{0.6}/\text{CNTs}$ is a promising catalyst for the production of hydrogen from hydrazine hydrolysate.

Cheng et al. [102] reported a simple Ni-Pt-MnOx synthesis method to support nitrogen-doped porous carbon (NPC) from annealed metal-organic skeleton MOFs at different temperatures in Ar. Interestingly, the produced $(\text{Ni}_3\text{Pt}_7)_{0.5}-(\text{MnOx})_{0.5}/\text{NPC-900}$ exhibitors showed better catalytic activity for the dehydrogenation of hydrazine in alkaline solution, with primary turnover frequencies of 706 and 120 h^{-1} at 323 K and ordinary temperature, respectively. Because of the synergistic electronic effect of Ni-Pt and MnOx and the small-scale size and lofty dispersion of the Ni-Pt-MnOx nano-catalyst, NPC, as an excellent carrier, may have excellent catalytic performance, large pore volume, high specific surface area, high nitrogen content and conductivity, and the high density of metal-n active sites between Ni-Pt-MnOx and NPC. As shown in Figure 11, the presence of OH^- limits the formation of undesirable

N_2H_5^+ in aqueous solutions and promotes the cleavage of the N–H bond during the determination of the hydrazine dehydrogenation reaction. The decomposition of $(\text{Ni}_3\text{Pt}_7)_{0.5}-(\text{MnOx})_{0.5}/\text{NPC-900}$ in alkaline solution may be concerned with the following steps: first, target N_2H_4 adsorption may be intensified due to the illustrious surface area and porosity of NPC-900; second, N_2H_4 decomposition into N_2 and H_2 , the rate of desorption of N_2 and H_2 molecules generated; third, desorption of the resultant N_2 and H_2 molecules as shown in Figure 11. Furthermore, the charge transfer process was involved in the above three steps, which can be promoted by the NPC-900 porous network with high conductivity and graphitization, as well as the introduction of nitrogen atoms and MnOx. This can explain the splendid catalytic performance of $(\text{Ni}_3\text{Pt}_7)_{0.5}-(\text{MnOx})_{0.5}/\text{NPC-900}$ catalyst.



Scheme 6. Illustration of the synthesis process of Ni-Pt/carbon nanotubes (CNTs); copyright (2019), Wiley.

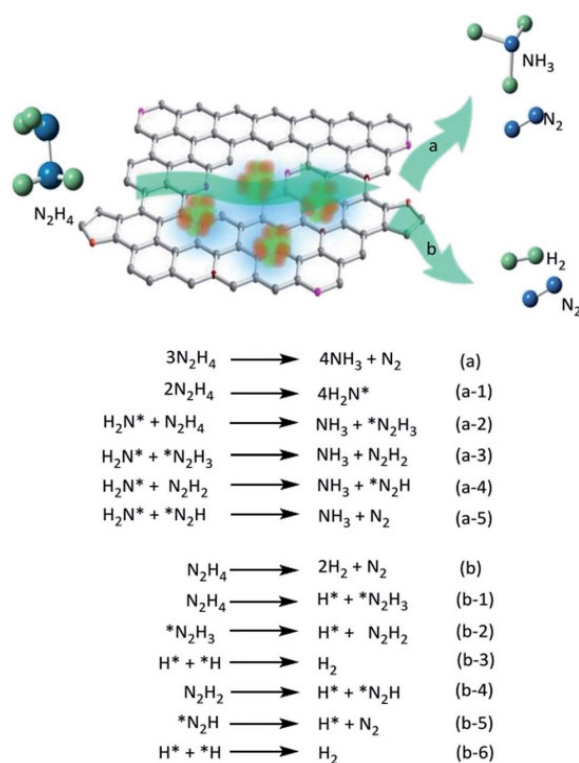


Figure 11. The possible mechanism of decomposition of hydrazine catalyzed by $(\text{Ni}_3\text{Pt}_7)_{0.5}-(\text{MnOx})_{0.5}/\text{NPC-900}$ in the absence of NaOH (pathway a) and in the presence of NaOH (pathway b); copyright (2016), *Journal of Materials Chemistry A*.

6.7. Summary

Chemical hydrogen storage materials need to be efficiently catalyzed by a suitable catalyst to release hydrogen efficiently over a wide temperature range and to meet environmental standards [103]. The research results show that hydrous hydrazine can meet the above requirements. The developed Pt-based catalysts mainly include Ni-Pt alloy catalysts [104], Ni-Pt-supported catalysts [105], and Ni-Pt-YOx-supported multi-metal catalysts [102]. Among them, Ni-Pt-supported catalysts and Ni-Pt-YOx-supported multi-metal catalysts have high practicality. The Ni-Pt alloy effect, the strong interaction between Ni-Pt and the support, and the synergistic effect between the metal oxide and Ni-Pt are the reasons for the high activity and hydrogen selectivity of the catalyst. In the future, the development direction of catalysts will tend to be low-cost, low reaction temperature, and low operating costs to meet the needs of large-scale hydrous hydrazine catalytic hydrogen production. On the one hand, the presence of Pt and Ni in the Pt-Ni alloy state is an important factor for the high activity of the catalyst; on the other hand, the carrier rGO also plays a supporting and synergistic role, making the hydrazine molecule preferentially break the N–H bond on the catalyst surface to promote the decomposition reaction to proceed completely [106]. The introduction of metal Ce can significantly improve the catalytic activity and hydrogen selectivity of the catalyst to catalyze the decomposition of hydrous hydrazine to produce hydrogen. The study also found that only the proper amount of Ce can be introduced to ensure the high activity of the catalyst, the high dispersion of Ni-Pt-CeOx, and the strong interaction between Ni-Pt-CeOx and the support. The excellent activity of the catalyst is due to the synergistic electronic effect between Ni-Pt alloy particles and MnOx.

7. Conclusions

The research progress of Pt-based catalysts for catalytic hydrogen production from hydrous hydrazine decomposition is reviewed. The decomposition of hydrous hydrazine includes two ways: complete decomposition and incomplete decomposition. Its hydrogen content is as high as 8.0 wt%, which has a good application prospect. Pt-based catalysts play an important role in catalyzing the selective decomposition of hydrous hydrazine to produce hydrogen. They are mainly divided into Pt-support catalysts, Pt-Ni alloy catalysts, Pt-Ni-supports catalysts, and Pt-Ni-YOx-support multi-metal catalysts (Y is Mn, Ce). Due to the synergistic effect between the metal oxides YOx and Pt-Ni, and the strong interaction between the metal or metal composite and the carrier, the Ni-based catalyst exhibits high catalytic activity and has a good effect on hydrogen in the production of hydrous hydrazine 100% selectivity. In addition, the existence of basic additives is helpful to improve the catalytic activity and selectivity of metal catalysts. We look forward to providing some reference for improving the hydrogen economy of the catalyst and other applications.

Author Contributions: Conceptualization, C.W.; writing—original draft preparation, L.Z., X.L., and M.Y.; writing—review and editing, M.Y., L.X., and C.W.; supervision, C.W. All authors have read and agreed to the published version of the manuscript.

Funding: This research was supported by Anhui Provincial Natural Science Foundation (1908085QB68), the Natural Science Foundation of the Anhui Higher Education Institutions of China (KJ2019A0072), Major Science and Technology Project of Anhui Province(201903a05020055), Foundation of Zhejiang Provincial Key Laboratory of Advanced Chemical Engineering Manufacture Technology (ZJKL-ACEMT-1802), China Postdoctoral Science Foundation (2019M662060,2020T130580), and the Research Fund for Young Teachers of Anhui University of Technology (QZ201610).

Conflicts of Interest: The authors declare no conflict of interest.

References

1. Cheng, Y.; Wu, X.; Xu, H. Catalytic decomposition of hydrous hydrazine for hydrogen production. *Sustain. Energy Fuels* **2019**, *3*, 343–365. [[CrossRef](#)]
2. Zhang, M.Y.; Xiao, X.; Wu, Y.; An, Y.; Xu, L.; Wan, C. Hydrogen Production from Ammonia Borane over PtNi Alloy Nanoparticles Immobilized on Graphite Carbon Nitride. *Catalysts* **2019**, *9*, 1009. [[CrossRef](#)]

3. Zhou, L.; Sun, L.; Xu, L.; Wan, C.; An, Y.; Ye, M. Recent Developments of Effective Catalysts for Hydrogen Storage Technology Using N-Ethylcarbazole. *Catalysts* **2020**, *10*, 648. [[CrossRef](#)]
4. Aranishi, K.; Singh, A.K.; Xu, Q. Dendrimer-Encapsulated Bimetallic Pt-Ni Nanoparticles as Highly Efficient Catalysts for Hydrogen Generation from Chemical Hydrogen Storage Materials. *ChemCatChem* **2013**, *5*, 2248–2252. [[CrossRef](#)]
5. Wang, J.; Zhang, X.B.; Wang, Z.L.; Wang, L.M.; Zhang, Y. Rhodium–nickel nanoparticles grown on graphene as highly efficient catalyst for complete decomposition of hydrous hydrazine at room temperature for chemical hydrogen storage. *Energy Environ. Sci.* **2012**, *5*, 6885–6888. [[CrossRef](#)]
6. Zhang, L.T.; Ji, L.; Yao, Z.D.; Yan, N.H.; Sun, Z.X.; Yang, L.; Zhu, X.Q.; Hu, S.L.; Chen, L.X. Facile synthesized Fe nanosheets as superior active catalyst for hydrogen storage in MgH₂. *Int. J. Hydrogen Energy* **2019**, *44*, 21955–21964. [[CrossRef](#)]
7. Liu, M.; Zhou, L.; Luo, X.; Wan, C.; Xu, L. Recent Advances in Noble Metal Catalysts for Hydrogen Production from Ammonia Borane. *Catalysts* **2020**, *10*, 788. [[CrossRef](#)]
8. He, L.; Huang, Y.; Wang, A.; Wang, X.; Chen, X.; Delgado, J.J.; Zhang, T. A Noble-Metal-Free Catalyst Derived from Ni–Al Hydrotalcite for Hydrogen Generation from N₂H₄·H₂O Decomposition. *Angew. Chem. Int. Ed.* **2012**, *51*, 6191–6194. [[CrossRef](#)]
9. Zhang, L.T.; Xiao, X.Z.; Chen, L.X.; Fan, X.L.; Zheng, J.G.; Huang, X. Correction for enhanced hydrogen storage properties of MgH₂ with numerous hydrogen diffusion channels provided by Na₂Ti₃O₇ nanotubes. *J. Mater. Chem. A* **2017**, *5*, 6178–6185. [[CrossRef](#)]
10. Wan, C.; Zhou, L.; Sun, L.; Xu, L.X.; Cheng, D.G.; Chen, F.Q.; Zhan, X.L.; Yang, Y.R. Boosting visible-light-driven hydrogen evolution from formic acid over AgPd/2D g-C₃N₄ nanosheets Mott-Schottky photocatalyst. *Chem. Eng. J.* **2020**, *396*, 125229. [[CrossRef](#)]
11. Singh, A.K.; Xu, Q. Metal–Organic Framework Supported Bimetallic Ni–Pt Nanoparticles as High-performance Catalysts for Hydrogen Generation from Hydrazine in Aqueous Solution. *ChemCatChem* **2013**, *5*, 3000–3004. [[CrossRef](#)]
12. Lin, J.; Chen, J.; Su, W. Rhodium–Cobalt Bimetallic Nanoparticles: A Catalyst for Selective Hydrogenation of Unsaturated Carbon–Carbon Bonds with Hydrous Hydrazine. *Adv. Synth. Catal.* **2013**, *355*, 41–46. [[CrossRef](#)]
13. Cao, N.; Su, J.; Luo, W.; Cheng, G. Ni–Pt nanoparticles supported on MIL-101 as highly efficient catalysts for hydrogen generation from aqueous alkaline solution of hydrazine for chemical hydrogen storage. *Int. J. Hydrogen Energy* **2014**, *39*, 9726–9734. [[CrossRef](#)]
14. Song, X.; Yang, P.; Wang, J.; Zhao, X.; Zhou, Y.; Li, Y.; Yang, L. NiFePd/UiO-66 nanocomposites as highly efficient catalysts to accelerate hydrogen evolution from hydrous hydrazine. *Inorg. Chem. Front.* **2019**, *6*, 2727–2735. [[CrossRef](#)]
15. Wang, K.; Yao, Q.; Qing, S.; Lu, Z.H. La (OH)₃ nanosheet-supported CoPt nanoparticles: A highly efficient and magnetically recyclable catalyst for hydrogen production from hydrazine in aqueous solution. *J. Mater. Chem. A* **2019**, *7*, 9903–9911. [[CrossRef](#)]
16. Chen, J.; Zou, H.; Yao, Q.; Luo, M.; Li, X.; Lu, Z.H. Cr₂O₃-modified NiFe nanoparticles as a noble-metal-free catalyst for complete dehydrogenation of hydrazine in aqueous solution. *Appl. Surf. Sci.* **2020**, *501*, 144247. [[CrossRef](#)]
17. Chen, J.; Lu, Z.H.; Huang, W.; Kang, Z.; Chen, X. Galvanic replacement synthesis of NiPt/graphene as highly efficient catalysts for hydrogen release from hydrazine and hydrazine borane. *J. Alloys Compd.* **2017**, *695*, 3036–3043. [[CrossRef](#)]
18. Zhong, D.C.; Mao, Y.L.; Tan, X.; Zhong, P.; Liu, L.X. RhNi nanocatalyst: Spontaneous alloying and high activity for hydrogen generation from hydrous hydrazine. *Int. J. Hydrogen Energy* **2016**, *41*, 6362–6368. [[CrossRef](#)]
19. Song-Il, O.; Yan, J.M.; Wang, H.L.; Wang, Z.L.; Jiang, Q. High catalytic kinetic performance of amorphous CoPt NPs induced on CeO_x for H₂ generation from hydrous hydrazine. *Int. J. Hydrogen Energy* **2014**, *39*, 3755–3761. [[CrossRef](#)]
20. Al-Thubaiti, K.S.; Khan, Z. Trimetallic nanocatalysts to enhanced hydrogen production from hydrous hydrazine: The role of metal centers. *Int. J. Hydrogen Energy* **2020**, *45*, 13960–13974. [[CrossRef](#)]
21. Lu, Z.H.; Xu, Q. Recent progress in boron-and nitrogen-based chemical hydrogen storage. *Funct. Mater. Lett.* **2012**, *5*, 1230001. [[CrossRef](#)]

22. Manukyan, K.V.; Cross, A.; Rouvimov, S.; Miller, J.; Mukasyan, A.S.; Wolf, E.E. Low temperature decomposition of hydrous hydrazine over FeNi/Cu nanoparticles. *Appl. Catal. A Gen.* **2014**, *476*, 47–53. [[CrossRef](#)]
23. Tong, D.G. Retraction: Monodisperse Ni₃Fe single-crystalline nanospheres as a highly efficient catalyst for the complete conversion of hydrous hydrazine to hydrogen at room temperature. *J. Mater. Chem. A* **2019**, *7*, 20442. [[CrossRef](#)]
24. Dai, H.; Qiu, Y.P.; Dai, H.B.; Wang, P. A study of degradation phenomenon of Ni–Pt/CeO₂ catalyst towards hydrogen generation from hydrous hydrazine. *Int. J. Hydrogen Energy* **2017**, *42*, 16355–16361. [[CrossRef](#)]
25. Tong, D.G.; Chu, W.; Wu, P.; Gu, G.F.; Zhang, L. Mesoporous multiwalled carbon nanotubes as supports for monodispersed iron–boron catalysts: Improved hydrogen generation from hydrous hydrazine decomposition. *J. Mater. Chem. A* **2013**, *1*, 358–366. [[CrossRef](#)]
26. Wang, H.L.; Yan, J.M.; Li, S.J.; Zhang, X.W.; Jiang, Q. Noble-metal-free NiFeMo nanocatalyst for hydrogen generation from the decomposition of hydrous hydrazine. *J. Mater. Chem. A* **2014**, *3*, 121–124. [[CrossRef](#)]
27. Jiang, Y.; Kang, Q.; Zhang, J.; Dai, H.B.; Wang, P. High-performance nickel–platinum nanocatalyst supported on mesoporous alumina for hydrogen generation from hydrous hydrazine. *J. Power Source* **2015**, *273*, 554–560. [[CrossRef](#)]
28. He, L.; Liang, B.; Li, L.; Yang, X.; Huang, Y.; Wang, A.; Zhang, T. Cerium-oxide-modified nickel as a non-noble metal catalyst for selective decomposition of hydrous hydrazine to hydrogen. *ACS Catal.* **2015**, *5*, 1623–1628. [[CrossRef](#)]
29. Wang, J.; Li, Y.; Zhang, Y. Precious-Metal-Free Nanocatalysts for Highly Efficient Hydrogen Production from Hydrous Hydrazine. *Adv. Funct. Mater.* **2014**, *24*, 7073–7077. [[CrossRef](#)]
30. Zhang, J.; Kang, Q.; Yang, Z.; Dai, H.; Zhuang, D.; Wang, P. A cost-effective NiMoB–La(OH)₃ catalyst for hydrogen generation from decomposition of alkaline hydrous hydrazine solution. *J. Mater. Chem. A* **2013**, *1*, 11623–11628. [[CrossRef](#)]
31. Kang, W.; Varma, A. Hydrogen generation from hydrous hydrazine over Ni/CeO₂ catalysts prepared by solution combustion synthesis. *Appl. Catal. B Environ.* **2018**, *220*, 409–416. [[CrossRef](#)]
32. Dai, H.; Zhong, Y.; Wang, P. Hydrogen generation from decomposition of hydrous hydrazine over Ni–Ir/CeO₂ catalyst. *Prog. Nat. Sci. Mater. Int.* **2017**, *27*, 121–125. [[CrossRef](#)]
33. Dai, H.; Dai, H.B.; Zhong, Y.J.; Kang, Q.; Sun, L.X.; Wang, P. Kinetics of catalytic decomposition of hydrous hydrazine over CeO₂-supported bimetallic Ni–Pt nanocatalysts. *Int. J. Hydrogen Energy* **2017**, *42*, 5684–5693. [[CrossRef](#)]
34. Firdous, N.; Janjua, N.K.; Qazi, I.; Wattoo, M.H.S. Optimal Co–Ir bimetallic catalysts supported on γ -Al₂O₃ for hydrogen generation from hydrous hydrazine. *Int. J. Hydrogen Energy* **2016**, *41*, 984–995. [[CrossRef](#)]
35. Xia, B.; Chen, K.; Luo, W.; Cheng, G. NiRh nanoparticles supported on nitrogen-doped porous carbon as highly efficient catalysts for dehydrogenation of hydrazine in alkaline solution. *Nano Res.* **2015**, *8*, 3472–3479. [[CrossRef](#)]
36. Kang, Q.; Wang, T.; Li, P.; Liu, L.; Chang, K.; Li, M.; Ye, J. Photocatalytic reduction of carbon dioxide by hydrous hydrazine over Au–Cu alloy nanoparticles supported on SrTiO₃/TiO₂ coaxial nanotube arrays. *Angew. Chem. Int. Ed.* **2015**, *54*, 841–845. [[CrossRef](#)]
37. Lin, W.; Cheng, H.; He, L.; Yu, Y.; Zhao, F. High performance of Ir-promoted Ni/TiO₂ catalyst toward the selective hydrogenation of cinnamaldehyde. *J. Catal.* **2013**, *303*, 110–116. [[CrossRef](#)]
38. Alberas, D.J.; Kiss, J.; Liu, Z.M.; White, J.M. Surface chemistry of hydrazine on Pt (111). *Surf. Sci.* **1992**, *278*, 51–61. [[CrossRef](#)]
39. Huang, S.X.; Rufael, T.S.; Gland, J.L. Diimide formation on the Ni (100) surface. *Surf. Sci. Lett.* **1993**, *290*, 673–676.
40. He, L.; Liang, B.; Huang, Y.; Zhang, T. Design strategies of highly selective nickel catalysts for H₂ production via hydrous hydrazine decomposition: A review. *Nat. Sci. Rev.* **2018**, *5*, 356–364. [[CrossRef](#)]
41. Batonneau, Y.; Kappenstein, C.J.; Keim, W. Catalytic decomposition of energetic compounds: Gas generators and propulsion. *Handb. Heterog. Catal. Online* **2008**, 2647–2676. [[CrossRef](#)]
42. Lucien, H.W. Thermal Decomposition of Hydrazine. *J. Chem. Eng. Data* **1961**, *6*, 584–586. [[CrossRef](#)]
43. Zheng, M.; Cheng, R.; Chen, X.; Li, N.; Li, L.; Wang, X.; Zhang, T. A novel approach for CO-free H₂ production via catalytic decomposition of hydrazine. *Int. J. Hydrogen Energy* **2005**, *30*, 1081–1089. [[CrossRef](#)]

44. Singh, S.K.; Xu, Q. Complete conversion of hydrous hydrazine to hydrogen at room temperature for chemical hydrogen storage. *J. Am. Chem. Soc.* **2009**, *131*, 18032–18033. [[CrossRef](#)]
45. Singh, S.K.; Zhang, X.B.; Xu, Q. Room-temperature hydrogen generation from hydrous hydrazine for chemical hydrogen storage. *J. Am. Chem. Soc.* **2009**, *131*, 9894–9895. [[CrossRef](#)]
46. Wan, C.; Sun, L.; Xu, L.; Cheng, D.G.; Chen, F.; Zhan, X.; Yang, Y. Novel NiPt alloy nanoparticle decorated 2D layered g-C₃N₄ nanosheets: A highly efficient catalyst for hydrogen generation from hydrous hydrazine. *J. Mater. Chem. A* **2019**, *7*, 8798–8804. [[CrossRef](#)]
47. Jiang, R.; Qu, X.; Zeng, F.; Li, Q.; Zheng, X.; Xu, Z.; Peng, J. MOF-74-immobilized ternary RhNiP nanoparticles as highly efficient hydrous hydrazine dehydrogenation catalysts in alkaline solutions. *Int. J. Hydrogen Energy* **2019**, *44*, 6383–6391. [[CrossRef](#)]
48. Qiu, Y.P.; Yin, H.; Dai, H.; Gan, L.Y.; Dai, H.B.; Wang, P. Tuning the Surface Composition of Ni/meso-CeO₂ with Iridium as an Efficient Catalyst for Hydrogen Generation from Hydrous Hydrazine. *Chem. A Eur. J.* **2018**, *24*, 4902–4908. [[CrossRef](#)]
49. Chen, J.; Yao, Q.; Zhu, J.; Chen, X.; Lu, Z.H. Rh–Ni nanoparticles immobilized on Ce (OH) CO₃ nanorods as highly efficient catalysts for hydrogen generation from alkaline solution of hydrazine. *Int. J. Hydrogen Energy* **2016**, *41*, 3946–3954. [[CrossRef](#)]
50. Kumar, P.; Kumar, A.; Queffélec, C.; Gudat, D.; Wang, Q.; Jain, S.L.; Szunerits, S. Visible light assisted hydrogen generation from complete decomposition of hydrous hydrazine using rhodium modified TiO₂ photocatalysts. *Photochem. Photobiol. Sci.* **2017**, *16*, 1036–1042. [[CrossRef](#)]
51. Wan, C.; Cheng, D.G.; Chen, F.Q.; Zhan, X.L. Fabrication of CeO₂ nanotube supported Pt catalyst encapsulated with silica for high and stable performance. *Chem. Commun.* **2015**, *51*, 9785–9788. [[CrossRef](#)]
52. Varma, A.; Mukasyan, A.S.; Rogachev, A.S.; Manukyan, K.V. Solution combustion synthesis of nanoscale materials. *Chem. Rev.* **2016**, *116*, 14493–14586. [[CrossRef](#)]
53. Baek, S.; Kim, K.H.; Kim, M.J.; Kim, J.J. Morphology control of noble metal catalysts from planar to dendritic shapes by galvanic displacement. *Appl. Catal. B Environ.* **2017**, *217*, 313–321. [[CrossRef](#)]
54. Ubeyitogullari, A.; Ciftci, O.N. Generating phytosterol nanoparticles in nanoporous bioaerogels via supercritical carbon dioxide impregnation: Effect of impregnation conditions. *J. Food Eng.* **2017**, *207*, 99–107. [[CrossRef](#)]
55. Li, S.; Adkins, N.J.; McCain, S.; Attallah, M.M. Suspended droplet alloying: A new method for combinatorial alloy synthesis; nitinol-based alloys as an example. *J. Alloys Compd.* **2018**, *768*, 392–398. [[CrossRef](#)]
56. Wu, Y.; Wang, D.; Zhou, G.; Yu, R.; Chen, C.; Li, Y. Sophisticated construction of Au islands on Pt–Ni: An ideal trimetallic nanoframe catalyst. *J. Am. Chem. Soc.* **2014**, *136*, 11594–11597. [[CrossRef](#)]
57. Fang, H.; Yang, J.; Wen, M.; Wu, Q. Nanoalloy materials for chemical catalysis. *Adv. Mater.* **2018**, *30*, 1705698. [[CrossRef](#)] [[PubMed](#)]
58. Zou, H.; Yao, Q.; Huang, M.; Zhu, M.; Zhang, F.; Lu, Z.H. Noble-metal-free NiFe nanoparticles immobilized on nano CeZrO₂ solid solutions for highly efficient hydrogen production from hydrous hydrazine. *Sustain. Energy Fuels* **2019**, *3*, 3071–3077. [[CrossRef](#)]
59. Yin, B.; Wang, Q.; Liu, T.; Gao, G. Anchoring ultrafine RhNi nanoparticles on titanium carbides/manganese oxide as an efficient catalyst for hydrogen generation from hydrous hydrazine. *New J. Chem.* **2018**, *42*, 20001–20006. [[CrossRef](#)]
60. Jiang, Y.Y.; Dai, H.B.; Zhong, Y.J.; Chen, D.M.; Wang, P. Complete and rapid conversion of hydrazine monohydrate to hydrogen over supported Ni–Pt nanoparticles on mesoporous ceria for chemical hydrogen storage. *Chem. A Eur. J.* **2015**, *21*, 15439–15445. [[CrossRef](#)]
61. Cho, J.; Lee, S.; Yoon, S.P.; Han, J.; Nam, S.W.; Lee, K.Y.; Ham, H.C. Role of heteronuclear interactions in selective H₂ formation from HCOOH decomposition on bimetallic Pd/M (M = late transition FCC metal) catalysts. *ACS Catal.* **2017**, *7*, 2553–2562. [[CrossRef](#)]
62. Cheng, M.; Wen, M.; Zhou, S.; Wu, Q.; Sun, B. Solvothermal synthesis of NiCo alloy icosahedral nanocrystals. *Inorg. Chem.* **2012**, *51*, 1495–1500. [[CrossRef](#)] [[PubMed](#)]
63. Chen, C.; Kang, Y.; Huo, Z.; Zhu, Z.; Huang, W.; Xin, H.L.; Snyder, J.D.; Li, D.; Herron, J.A.; Mavrikakis, M.; et al. Highly crystalline multimetallic nanoframes with three-dimensional electrocatalytic surfaces. *Science* **2014**, *343*, 1339–1343. [[CrossRef](#)] [[PubMed](#)]
64. Wu, Y.; Wang, D.; Niu, Z.; Chen, P.; Zhou, G.; Li, Y. A strategy for designing a concave Pt–Ni alloy through controllable chemical etching. *Angew. Chem. Int. Ed.* **2012**, *51*, 12524–12528. [[CrossRef](#)]

65. Yin, Y.; Rioux, R.M.; Erdonmez, C.K.; Hughes, S.; Somorjai, G.A.; Alivisatos, A.P. Formation of hollow nanocrystals through the nanoscale Kirkendall effect. *Science* **2004**, *304*, 711–714. [[CrossRef](#)]
66. Yadav, M.; Xu, Q. Liquid-phase chemical hydrogen storage materials. *Energy Environ. Sci.* **2012**, *5*, 9698–9725. [[CrossRef](#)]
67. Yang, H.; Lu, B.; Guo, L.; Qi, B. Cerium hexacyanoferrate/ordered mesoporous carbon electrode and its application in electrochemical determination of hydrous hydrazine. *J. Electroanal. Chem.* **2011**, *650*, 171–175. [[CrossRef](#)]
68. Song, F.Z.; Zhu, Q.L.; Xu, Q. Monodispersed PtNi nanoparticles deposited on diamine-alkalized graphene for highly efficient dehydrogenation of hydrous hydrazine at room temperature. *J. Mater. Chem. A* **2015**, *3*, 23090–23094. [[CrossRef](#)]
69. Yang, K.; Yang, K.; Zhang, S.; Luo, Y.; Yao, Q.; Lu, Z.H. Complete dehydrogenation of hydrazine borane and hydrazine catalyzed by MIL-101 supported NiFePd nanoparticles. *J. Alloys Compd.* **2018**, *732*, 363–371. [[CrossRef](#)]
70. Tong, D.G.; Tang, D.M.; Chu, W.; Gu, G.F.; Wu, P. Monodisperse Ni₃Fe single-crystalline nanospheres as a highly efficient catalyst for the complete conversion of hydrous hydrazine to hydrogen at room temperature. *J. Mater. Chem. A* **2013**, *1*, 6425–6432. [[CrossRef](#)]
71. Yang, P.; Yang, L.; Gao, Q.; Luo, Q.; Zhao, X.; Mai, X.; Yang, R. Anchoring carbon nanotubes and post-hydroxylation treatment enhanced Ni nanofiber catalysts towards efficient hydrous hydrazine decomposition for effective hydrogen generation. *Chem. Commun.* **2019**, *55*, 9011–9014. [[CrossRef](#)] [[PubMed](#)]
72. Wang, J.; Li, W.; Wen, Y.; Gu, L.; Zhang, Y. Rh-Ni-B nanoparticles as highly efficient catalysts for hydrogen generation from hydrous hydrazine. *Adv. Energy Mater.* **2015**, *5*, 1401879. [[CrossRef](#)]
73. Zhao, B.; Song, J.; Ran, R.; Shao, Z. Catalytic decomposition of hydrous hydrazine to hydrogen over oxide catalysts at ambient conditions for PEMFCs. *Int. J. Hydrogen Energy* **2012**, *37*, 1133–1139. [[CrossRef](#)]
74. Zhong, Y.; Dai, H.; Wang, P. Preparation of Ni-Pt/La₂O₃ catalyst and its kinetics study of hydrous hydrazine for hydrogen generation. *Acta Met. Sin.* **2015**, *52*, 505–512.
75. Bhattacharjee, D.; Mandal, K.; Dasgupta, S. High performance nickel–palladium nanocatalyst for hydrogen generation from alkaline hydrous hydrazine at room temperature. *J. Power Source* **2015**, *287*, 96–99. [[CrossRef](#)]
76. Bhattacharjee, D.; Dasgupta, S. Trimetallic NiFePd nanoalloy catalysed hydrogen generation from alkaline hydrous hydrazine and sodium borohydride at room temperature. *J. Mater. Chem. A* **2015**, *3*, 24371–24378. [[CrossRef](#)]
77. Zhang, Z.; Zhang, S.; Yao, Q.; Chen, X.; Lu, Z.H. Controlled synthesis of MOF-encapsulated NiPt nanoparticles toward efficient and complete hydrogen evolution from hydrazine borane and hydrazine. *Inorg. Chem.* **2017**, *56*, 11938–11945. [[CrossRef](#)]
78. Zhao, P.; Cao, N.; Su, J.; Luo, W.; Cheng, G. NiIr nanoparticles immobilized on the pores of MIL-101 as highly efficient catalyst toward hydrogen generation from hydrous hydrazine. *ACS Sustain. Chem. Eng.* **2015**, *3*, 1086–1093. [[CrossRef](#)]
79. He, L.; Huang, Y.; Wang, A.; Wang, X.; Zhang, T. H₂ production by selective decomposition of hydrous hydrazine over Raney Ni catalyst under ambient conditions. *AIChE J.* **2013**, *59*, 4297–4302. [[CrossRef](#)]
80. Wu, D.; Wen, M.; Lin, X.; Wu, Q.; Gu, C.; Chen, H. A NiCo/NiO–CoO_x ultrathin layered catalyst with strong basic sites for high-performance H₂ generation from hydrous hydrazine. *J. Mater. Chem. A* **2016**, *4*, 6595–6602. [[CrossRef](#)]
81. Xu, L.; Liu, N.; Hong, B.; Cui, P.; Cheng, D.G.; Chen, F.; Wan, C. Nickel–platinum nanoparticles immobilized on graphitic carbon nitride as highly efficient catalyst for hydrogen release from hydrous hydrazine. *RSC Adv.* **2016**, *6*, 31687–31691. [[CrossRef](#)]
82. Zhang, Z.; Zhang, S.; Yao, Q.; Feng, G.; Zhu, M.; Lu, Z.H. Metal–organic framework immobilized RhNi alloy nanoparticles for complete H₂ evolution from hydrazine borane and hydrous hydrazine. *Inorg. Chem. Front.* **2018**, *5*, 370–377. [[CrossRef](#)]
83. Zhu, Q.L.; Xu, Q. Liquid organic and inorganic chemical hydrides for high-capacity hydrogen storage. *Energy Environ. Sci.* **2015**, *8*, 478–512. [[CrossRef](#)]
84. Singh, S.K.; Singh, A.K.; Aranishi, K.; Xu, Q. Noble-metal-free bimetallic nanoparticle-catalyzed selective hydrogen generation from hydrous hydrazine for chemical hydrogen storage. *J. Am. Chem. Soc.* **2011**, *133*, 19638–19641. [[CrossRef](#)]

85. Singh, S.K.; Xu, Q. Bimetallic Ni–Pt nanocatalysts for selective decomposition of hydrazine in aqueous solution to hydrogen at room temperature for chemical hydrogen storage. *Inorg. Chem.* **2010**, *49*, 6148–6152. [[CrossRef](#)]
86. Singh, S.K.; Lu, Z.H.; Xu, Q. Temperature-induced enhancement of catalytic performance in selective hydrogen generation from hydrous hydrazine with Ni-based nanocatalysts for chemical hydrogen storage. *Eur. J. Inorg. Chem.* **2011**, *2011*, 2232–2237. [[CrossRef](#)]
87. Singh, A.K.; Yadav, M.; Aranishi, K.; Xu, Q. Temperature-induced selectivity enhancement in hydrogen generation from Rh–Ni nanoparticle-catalyzed decomposition of hydrous hydrazine. *Int. J. Hydrogen Energy* **2012**, *37*, 18915–18919. [[CrossRef](#)]
88. Guo, F.; Zou, H.; Yao, Q.; Huang, B.; Lu, Z.H. Monodispersed bimetallic nanoparticles anchored on TiO₂-decorated titanium carbide MXene for efficient hydrogen production from hydrazine in aqueous solution. *Renew. Energy* **2020**, *155*, 1293–1301. [[CrossRef](#)]
89. Men, Y.; Su, J.; Wang, X.; Cai, P.; Cheng, G.; Luo, W. NiPt nanoparticles supported on CeO₂ nanospheres for efficient catalytic hydrogen generation from alkaline solution of hydrazine. *Chin. Chem. Lett.* **2019**, *30*, 634–637. [[CrossRef](#)]
90. Shi, Q.; Qiu, Y.P.; Dai, H.; Wang, P. Study of formation mechanism of Ni–Pt/CeO₂ catalyst for hydrogen generation from hydrous hydrazine. *J. Alloys Compd.* **2019**, *787*, 1187–1194. [[CrossRef](#)]
91. Dai, H.; Qiu, Y.P.; Dai, H.B.; Wang, P. Ni–Pt/CeO₂ loaded on granular activated carbon: An efficient monolithic catalyst for controlled hydrogen generation from hydrous hydrazine. *ACS Sustain. Chem. Eng.* **2018**, *6*, 9876–9882. [[CrossRef](#)]
92. He, L.; Huang, Y.; Wang, A.; Liu, Y.; Liu, X.; Chen, X.; Zhang, T. Surface modification of Ni/Al₂O₃ with Pt: Highly efficient catalysts for H₂ generation via selective decomposition of hydrous hydrazine. *J. Catal.* **2013**, *298*, 1–9. [[CrossRef](#)]
93. Kumar, A.; Yang, X.; Xu, Q. Ultrafine bimetallic Pt–Ni nanoparticles immobilized on 3-dimensional N-doped graphene networks: A highly efficient catalyst for dehydrogenation of hydrous hydrazine. *J. Mater. Chem. A* **2019**, *7*, 112–115. [[CrossRef](#)]
94. Zou, H.; Zhang, S.; Hong, X.; Yao, Q.; Luo, Y.; Lu, Z.H. Immobilization of Ni–Pt nanoparticles on MIL-101/rGO composite for hydrogen evolution from hydrous hydrazine and hydrazine borane. *J. Alloys Compd.* **2020**, *835*, 155426. [[CrossRef](#)]
95. Song, F.Z.; Yang, X.; Xu, Q. Ultrafine bimetallic Pt–Ni nanoparticles achieved by metal–organic framework templated zirconia/porous carbon/reduced graphene oxide: Remarkable catalytic activity in dehydrogenation of hydrous hydrazine. *Small Methods* **2020**, *4*, 1900707. [[CrossRef](#)]
96. Du, Y.; Su, J.; Luo, W.; Cheng, G. Graphene-supported nickel–platinum nanoparticles as efficient catalyst for hydrogen generation from hydrous hydrazine at room temperature. *ACS Appl. Mater. Interfaces* **2015**, *7*, 1031–1034. [[CrossRef](#)]
97. Zhong, Y.J.; Dai, H.B.; Zhu, M.; Wang, P. Catalytic decomposition of hydrous hydrazine over NiPt/La₂O₃ catalyst: A high-performance hydrogen storage system. *Int. J. Hydrogen Energy* **2016**, *41*, 11042–11049. [[CrossRef](#)]
98. Zhong, Y.J.; Dai, H.B.; Jiang, Y.Y.; Chen, D.M.; Zhu, M.; Sun, L.X.; Wang, P. Highly efficient Ni@ Ni–Pt/La₂O₃ catalyst for hydrogen generation from hydrous hydrazine decomposition: Effect of Ni–Pt surface alloying. *J. Power Source* **2015**, *300*, 294–300. [[CrossRef](#)]
99. Sun, J.K.; Xu, Q. Metal nanoparticles immobilized on carbon nanodots as highly active catalysts for hydrogen generation from hydrazine in aqueous solution. *ChemCatChem* **2015**, *7*, 526–531. [[CrossRef](#)]
100. Qiu, Y.P.; Shi, Q.; Zhou, L.L.; Chen, M.H.; Chen, C.; Tang, P.P.; Wang, P. NiPt Nanoparticles Anchored onto Hierarchical Nanoporous N-Doped Carbon as an Efficient Catalyst for Hydrogen Generation from Hydrazine Monohydrate. *ACS Appl. Mater. Interfaces* **2020**, *12*, 18617–18624. [[CrossRef](#)]
101. Zhang, M.; Liu, L.; Lu, S.; Xu, L.; An, Y.; Wan, C. Facile Fabrication of NiPt/CNTs as an Efficient Catalyst for Hydrogen Production from Hydrous Hydrazine. *Chem. Sel.* **2019**, *4*, 10494–10500. [[CrossRef](#)]
102. Xia, B.; Liu, T.; Luo, W.; Cheng, G. NiPt–MnO_x supported on N-doped porous carbon derived from metal–organic frameworks for highly efficient hydrogen generation from hydrazine. *J. Mater. Chem. A* **2016**, *4*, 5616–5622. [[CrossRef](#)]
103. Singh, S.K.; Xu, Q. Bimetallic nickel-iridium nanocatalysts for hydrogen generation by decomposition of hydrous hydrazine. *Chem. Commun.* **2010**, *46*, 6545–6547. [[CrossRef](#)]

104. Du, X.; Du, C.; Cai, P.; Luo, W.; Cheng, G. NiPt Nanocatalysts Supported on Boron and Nitrogen Co-Doped Graphene for Superior Hydrazine Dehydrogenation and Methanol Oxidation. *ChemCatChem* **2016**, *8*, 1410–1416. [[CrossRef](#)]
105. Wang, C.; Wang, H.L.; Gao, D.W.; Zhao, Z.K. Amorphous NiCoPt/Ce₂O₃ Nanoparticles as Highly Efficient Catalyst for Hydrogen Generation from Hydrous Hydrazine. *Mater. Sci. Forum* **2017**, *898*, 1862–1870. [[CrossRef](#)]
106. Kang, W.; Guo, H.; Varma, A. Noble-metal-free NiCu/CeO₂ catalysts for H₂ generation from hydrous hydrazine. *Appl. Catal. B Environ.* **2019**, *249*, 54–62. [[CrossRef](#)]



© 2020 by the authors. Licensee MDPI, Basel, Switzerland. This article is an open access article distributed under the terms and conditions of the Creative Commons Attribution (CC BY) license (<http://creativecommons.org/licenses/by/4.0/>).